Geopersia 2023, 13(1): 167-184
DOI: 10.22059/GEOPE.2023.350393.648684

RESEARCH PAPER

U-Pb Geochronological and Geochemical Characteristics of the Kalateh-Naser Intrusive Rocks, Eastern Lut, Iran

Maryam Sadat Mazhari [1], Saeed Saadat [2, *], Seyed Ahmad Mazaheri [1], Seyed Masoud Homam [1], Petrus Le Roux [3]

[1] Department of Geology, Faculty of Sciences, Ferdowsi University of Mashhad, Mashhad, Iran
[2] Department of Petroleum Engineering and Geology, Mashhad Branch, Islamic Azad University, Mashhad, Iran
[3] Department of Geological Sciences, University of Cape Town, South Africa

Received: 27 October 2022, Revised: 15 January 2023, Accepted: 16 January 2023
© University of Tehran

Abstract
The Kalateh-Naser area is located in the northeast of the Lut block (Eastern Iran). The rock units of the region generally include Cretaceous limestone units and metamorphosed carbonate rocks. Intrusive rocks emplaced in the study area are mainly composed of quartz monzonite, monzodiorite, quartz diorite, and granodiorite. These rocks are typically I-type with strongly metaluminous signatures. Dating using the zircon U-Pb method on two intrusive rocks revealed ages between 104.23 ± 0.85 Ma and 102.13 ± 0.91 Ma. Rb-Sr and Sm-Nd isotopic data yield mantle derived magma modified by the addition of crustal materials, as shown by initial $^{87}Sr/^{86}Sr$ ratios (0.7049 - 0.7051) and $^{143}Nd/^{144}Nd$ ratios (0.512697 - 0.512796). The geochemical compositions indicate enrichment of LILE compared to HFSE with $(La/Yb)_N$ values of 2.61–8.43. The LREE versus HREE ratios, as well as depletion of Nb, Ta and Ti elements in these intrusive rocks represent the characteristics of the rocks belonging to the subduction zone. The subduction characteristics of these rocks can be attributed to the subduction inherited in this part of eastern Iran. The whole-rock geochemistry combined with the Nd and Sr isotopic data and similar ages suggest that quartz monzonite and granodiorite are more likely co-magmatic and fall in VAG category. Comparing isotopic composition variations of the Kalateh-Naser rocks with other intrusive rocks from the Lut block, indicates a heterogeneous mantle beneath the Lut block and different amount of the metasomatized mantle source in eastern Iran.

Keywords: Kalateh-Naser Area, Iran, Zircon U-Pb Dating, Sr and Nd Isotopes.

Introduction

Eastern Iran including the Lut block as a micro-continental block has undergone various episodes of tectonic processes, magmatic pulses, various rotations and lateral movements from early Paleozoic to present (e.g., Berberian & King, 1981; Shahabpour, 2005). These events occurred due to the northeastward Arabian plate movement, northwestward movement of the Indian plate, and subduction of the oceanic lithosphere of the Oman Sea beneath the Makran region (Berberian & King, 1981; Saadat & Stern, 2011).

Volcanic rocks in the Lut block are mainly related to Eocene magmatic activities (e.g., Saadat & Stern, 2016), but the age of plutonic rocks which are rarely exposed in the Lut block still are poorly-known.

According to the available geochronology data, the Shahkuh granitoids in the southern part

* Corresponding author e-mail: saeed.saadat@colorado.edu

of the Lut block belong to the Late Jurrassic (Esmaiely et al., 2005). Early and Late Cretaceous plutonic rocks were reported in some location from Eastern Iran such as Kajeh (Najafi et al., 2014), Bajestan (Ahmadirouhani et al., 2017), Gazu (Mahdavi et al., 2016) and Kalate-Ahani (Karimpour et al., 2014).

Widespread magmatic activity in the Lut Block, is spatially and temporally associated with several types of mineralization events in form of Fe-skarn (e.g., Nejatzadeh et al., 2016; Karimpour et al., 2014), Cu-porphyry (e.g., Malekzadeh et al., 2015, Arjmandzadeh & Santos, 2014), and many other precious- and base-metal deposits (e.g., Abdi & Karimpour, 2013, Miri-Beydokhti et al., 2015).

To date, there has been insufficient geochronological data on Cretaceous plutonic rocks in the Lut block to distinctly recognize a temporal pattern. Data presented here can contribute to better understanding of the Mid-Cretaceous magmatism in the Lut block.

The main purpose of this paper is to present new geochemical and radiogenic isotopes data as well as chronological data for intrusive rocks from the Kalateh-Naser area, which is located in the northeastern part of the Lut block to find the petrogenesis of these plutonic rocks in this tectonically complex area.

Geological background

Limited geochronological data related to the Lut block indicate that magmatic activity was initiated in the Late Jurassic (Esmaiely et al., 2005) and had carried on into the Quaternary, resulting in different types of volcanic and subvolcanic stocks, plutonic rocks and associated mineralization processes.

Variations in the intensity of magmatic activity in the Lut block were also reported by Saadat and Stern (2016). Multiple theories of magmatic activities in the Lut block, especially during the Eocene, include eastward subduction of Sistan ocean toward the Afghan Block (e.g. Tirrul et al., 1983); eastward intra-oceanic subduction (Saccani et al., 2010); concurrent eastward and westward subduction (Arjmandzadeh et al., 2011), western oceanic subduction toward the Lut Block (Zarrinkoub et al., 2012); and asthenospheric upwelling (Pang et al., 2013). The peak magmatism activity (Eocene) in the Lut block is the result of the changes in the angle of the subduction of Neotethys oceanic crust, closing of Neotethys, and hot asthenosphere replacing the thinned lithospheric mantle beneath the Lut block (Saadat & Stern, 2016). Neogene and quaternary sedimentary deposits, consisting of salt flats, and alluvial fans and desert sand cover a vast area of the block, particularly in the south.

The Kalateh-Naser area is located in the northeast of the Lut block. Cretaceous carbonate rocks are the most abundant rock units in the study area (Fig. 1), turning to shale and thin bedded limestone and white crystalline limestone towards the west. Monzodiorite, quartz-monzonite, quartz-diorite and granodiorite are observed in the central part of the area. Based on structural control, as well as tectonic activity, only limited outcrop of recrystallized limestone and low-grade metamorphic rocks are present in the margins of intrusive igneous bodies in this area (Fig. 1 & 2).

Material and Methods

Major and trace elements geochemistry

Major and trace elements determination were conducted for nine selected unaltered samples. The samples were powdered (0.2 gr) and were fused using lithium metaborate/tetraborate flux and were then digested by nitric acid. Major elements analysis was done by XRF spectrometer (Phillips PW 1480 model), while trace and rare earth element analysis were done by Inductively

Coupled Plasma- Mass Spectrometry (ICP-MS) at the ACME Analytical Laboratories, Canada (Table 1).

Geochronology

Zircon U-Pb age dating was carried out for two rock samples from quartz monzonite and hornblende-pyroxene granodiorite. Roughly, 5 kg of rock of each sample was crushed to <400 *μm* in size. The zircon minerals were manually picked from the heavy mineral concentrate using a microscope, followed by placement on double sided sticky tape and epoxy glue to be poured into a 2.5 cm diameter mound on top of the zircons. An agilent 7500cs quadruple ICP-MS with a 193 nm Coherent Ar-F gas laser and Resonetics S155 ablation cell was utilized for sample analysis at the University of Arizona, USA. Table 2 illustrates the results of these analysis.

Rb–Sr and Sm–Nd isotopic analysis

Two unaltered samples of intrusive rocks were used for Rb–Sr and Sm–Nd isotopic analysis. The samples were powdered using an agate mortar. MC-ICP-MS laboratory of the Department of Geological Sciences, University of Cape Town, South Africa was utilized to perform Sr and Nd isotopic compositions. Approximately 50 mg of each of the samples were dissolved with ±5 ml of 4:1 concentrated HF:HNO_3 in closed Savillex beakers at 140ºC for 48 hours.

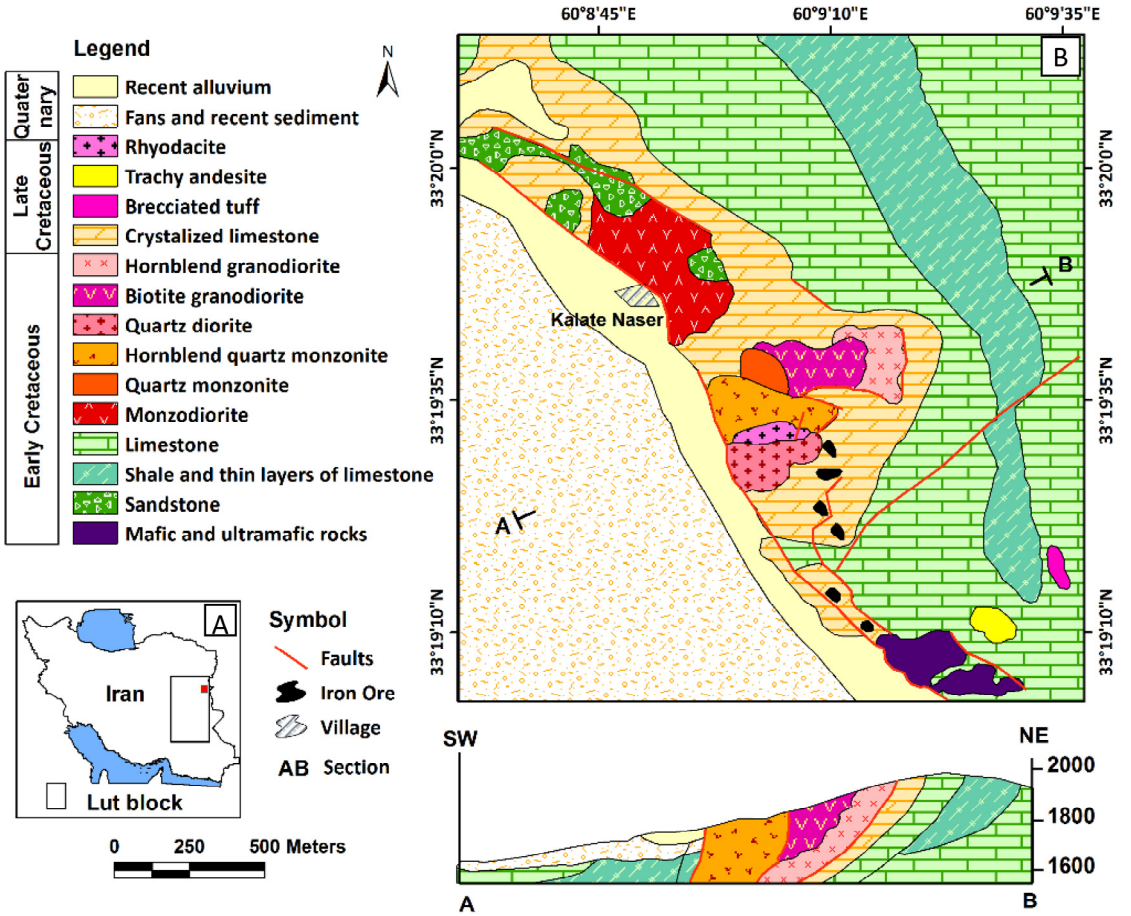

Figure 1. (A) Modified geological sketch map of Iran (after Berberian and King, 1981). The Square indicates the location of Kalateh-Naser comparing to Lut block. (B) Geological map of the Kalateh-Naser area

The completely digested samples were dried down, redissolved in a concentrated HNO_3, and this process repeated. Consequent to the final solution evaporating, samples get dissolved in 1.5 ml of 2M HNO_3 to become ready for column separation chemistry. The elements of interest, Sr and Nd, were isolated using sequential, stacked columns of Triskem Sr.Spec, TRU.Spec and Ln.Spec, modified after Pin et al., (2014).

Table 1. Whole-rock major (Wt. %) and trace element (ppm) compositions of the Kalateh-Naser intrusive rocks

Sample	M34	M98	M35	M33	M130	M102	M49	M62	M56
X	60°14'98"	60°15'17"	60°15'27"	60°15'97"	60°14'99"	60°15'11"	60°16'15"	60°15'18"	60°15'10"
Y	33°32'18"	33°32'47"	33°32'55"	33°32'54"	33°32'42"	33°32'59"	33°32'52"	33°32'98"	33°32'58"
Rock Type	Px Monzodiorite		Px-Hlb-Qtz Monzonite	Hlb Quartz Monzonite	Hlb-Px Granodiorite		Granodiorite		Qtz Diorite
SiO_2	53.51	52.79	59.32	57.29	67.12	69.6	63.75	64.7	55.73
TiO_2	0.8	0.78	0.66	0.68	0.43	0.42	0.51	0.35	0.7
Al_2O_3	14.15	16.21	16.3	18.59	14.72	13.5	15.94	13.88	17.9
FeO_t	7.49	7.1	5.56	5.78	3.64	3.23	3.91	2.94	6.01
MnO	0.08	0.26	0.08	0.1	0.06	0.07	0.06	0.08	0.11
MgO	4.64	4.43	2.92	2.49	1.29	1.68	1.38	1.07	2.75
CaO	7.21	9.3	7.98	7.78	3.39	3.26	3.78	3.17	8.1
Na_2O	4.68	3.59	3.63	3.55	3.47	4.2	3.88	3.43	3.36
K_2O	3.59	3.53	0.92	0.57	3.04	2.47	2.78	2.65	0.52
P_2O_5	0.08	0.26	0.08	0.1	0.06	0.07	0.06	0.08	0.11
Total	96.75	100.35	98.45	99.33	98.77	93.6	97.86	93.76	97.87
LOI	1.18	1.1	1.75	1.58	1.01	0.92	1.25	1	1.82
Ba	302	606.7	32	43.1	567.8	405	474.6	380.6	62
Rb	95	98.6	39	18	64.1	67	62.9	79.6	17
Sr	472	607.2	492	461.2	278.3	293	368.3	265.6	504.9
Zr	110	104	92	94	146	171	190	133	83
Nb	1	3.6	1	1.7	7.9	7	9.5	9	2.2
Co	23	24	16	13.2	8.8	9	9.4	8.1	13.9
La	15.7	15.5	6.5	6.8	20.4	21	17.7	23	8
Ce	29	28.6	11.8	12.5	39	39	33.7	40.2	15.1
Pr	3.87	3.92	2.33	2.25	5.02	4.98	4.55	4.74	2.64
Nd	15.9	15.7	10.6	10.4	18.9	18.5	17.8	16.4	12.1
Sm	3.63	3.54	2.82	2.77	3.67	3.81	3.75	2.98	3.26
Eu	1.18	1.07	0.88	0.94	0.86	0.92	0.93	0.76	1.07
Gd	3.41	3.36	2.78	2.81	3.2	3.71	3.42	2.92	3.38
Tb	0.52	0.54	0.44	0.42	0.54	0.56	0.58	0.44	0.53
Dy	2.99	3.14	2.5	2.76	3.37	3.1	3.57	2.61	3.39
Ho	0.75	0.66	0.64	0.55	0.68	0.69	0.73	0.54	0.74
Er	1.99	2.08	1.58	1.68	2.14	2.19	2.29	1.62	2.06
Tm	0.34	0.3	0.22	0.26	0.32	0.33	0.36	0.24	0.32
Yb	2.11	2.05	1.68	1.64	2.26	2.33	2.42	1.84	1.94
Lu	0.32	0.3	0.26	0.24	0.35	0.33	0.38	0.28	0.3
Y	33	18.5	19	15	19.4	35	21	15.8	18.5
Cs	0.88	2.02	0.38	0.45	0.91	1.92	0.94	1.19	0.68
Ta	0.2	0.2	0.1	0.1	0.7	0.6	0.8	0.9	0.1
Hf	2.5	2.4	2.3	2.5	4.1	3.9	5.4	3.9	2.4
Th	1	2.08	0.99	1.62	8.46	4	8.24	13.32	3.89
U	0.89	0.98	0.29	0.36	1.4	1	1.75	2.64	0.49
K_2O/Na_2	0.61	0.6	0.75	0.89	0.97	0.82	0.98	0.97	0.85
$(La/Yb)_N$	5.02	5.1	2.61	2.8	6.09	6.08	4.93	8.43	2.78
Eu/Eu*	0.99	0.95	0.97	0.99	0.74	0.75	0.8	0.79	0.99

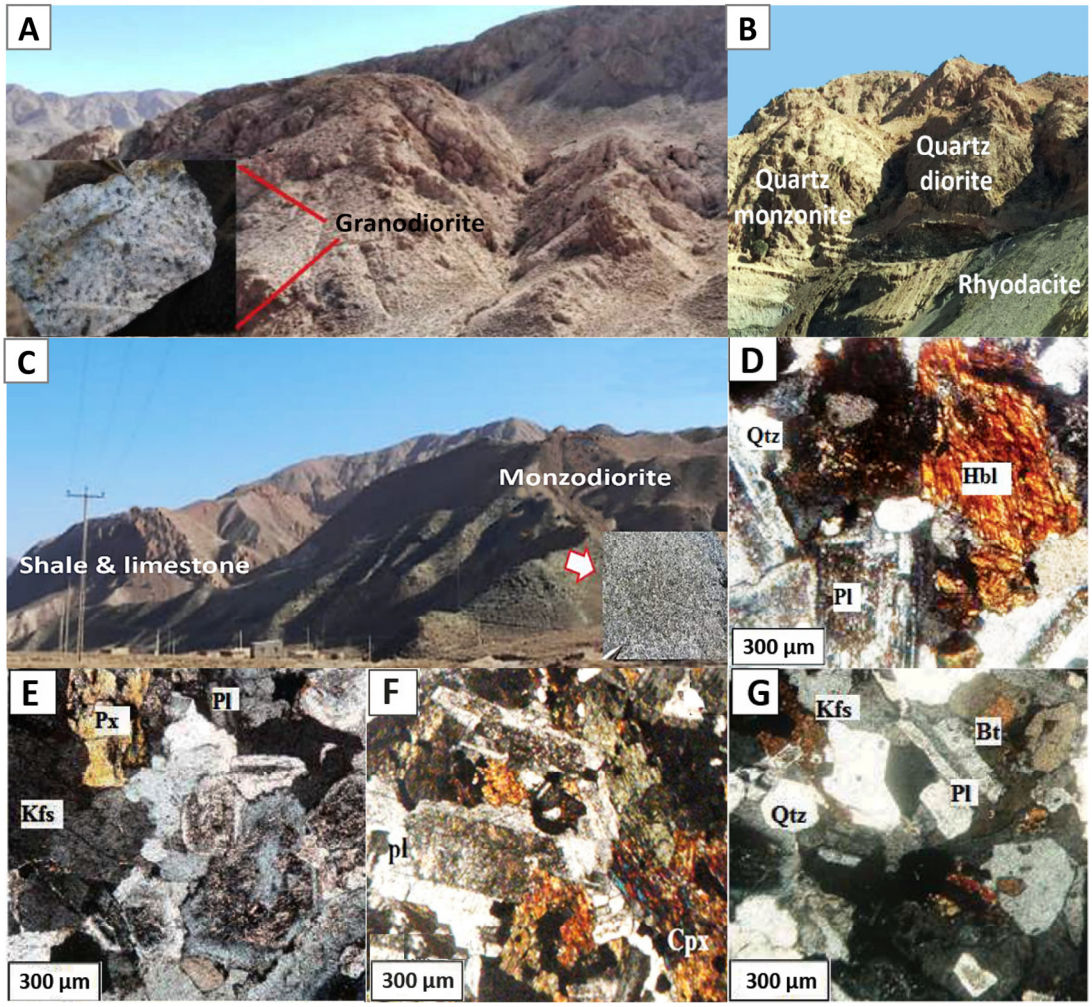

Figure 2. Outcrop of: (A) granodiorite (view to north-northeast). B) quartz monzonite and quartz diorite (view to east-southeast). (C) monzodiorite (view to north-northeast). Microphotographs of thin sections of intrusive rocks; (D) Hornblende quartz monzonite, (E) Monzodiorite, (F) Quartz diorite, (G) Biotite granodiorite. Hbl, hornblende; Bt, biotite; Kfs, K-feldspar; Qtz, quartz; Ep, epidote, Mgt, magnetite; Cpx, pyroxene (Mineral name abbreviations from Kretz, 1983)

The isolated Sr and Nd elemental fractions were analyzed utilizing a Nu Instruments NuPlamsa HR. Neodymium was analysed as 50 ppb 2% HNO_3 solutions additionally using a Nu Instruments DSN-100 desolvating nebulizer, with JNdi-1 as reference standard with the $^{143}Nd/^{144}Nd$ normalizing value of 0.512115 (Tanaka et al., 2000). Analysis of the international reference material BHVO-2 as unknown along with these samples yielded results ($^{87}Sr/^{86}Sr$ 0.703481 ±0.000010; $^{143}Nd/^{144}Nd$ 0.513004 ±0.000016) in agreement with long-term data from this facility ($^{87}Sr/^{86}Sr$ 0.703484 ±0.000039; $^{143}Nd/^{144}Nd$ 0.512986 ±0.000020; n > 290), as well as published data ($^{87}Sr/^{86}Sr$ 0.703469 ±0.000017; $^{143}Nd/^{144}Nd$ 0.512980 ±0.000012; GeoReM). Measured total procedural blanks were < 250 pg Sr and <50 pg Nd, therefore negligible. Table 3 presents the Rb–Sr and Sm–Nd isotope compositions.

Results

Field relationship and petrography

The geological units of this area can be divided into different groups (Fig. 1). Sandstone and

shales belonging to the Cretaceous, which are the oldest sedimentary units in the study area. Cream-colored limestone units that have the most outcrops in the area. Volcanic rocks (Late Cretaceous) with rhyodacite and trachyandesite composition has small outcrops in southern part of study area (Fig. 1).

Table 2. Zircon U-Pb age dating from the Kalateh-Naser area samples

Analysis	^{238}U	$^{235}U/^{207}Pb$	(%)±	$^{207}Pb/^{206}Pb$	(%)±	$^{238}U/^{206}Pb$	(%)±	$^{206}Pb/^{238}U$	(%)±	Best age (Ma)	± (Ma)
M33 (Quartzmonzonite)											
M-1	49	0.0953	2.4	22.6159	2.1	0.0156	1.2	100.0	1.2	100.0	1.2
M-2	64	0.0970	3.1	22.6254	2.8	0.0159	1.3	101.8	1.4	101.8	1.4
M-3	57	0.1041	2.8	21.1176	2.3	0.0160	1.6	102.0	1.6	102.0	1.6
M-4	81	0.1021	2.1	21.6166	1.7	0.0160	1.3	102.4	1.3	102.4	1.3
M-5	60	0.1033	2.0	21.4670	1.6	0.0161	1.1	102.9	1.1	102.9	1.1
M-6	50	0.1067	2.0	20.8054	1.6	0.0161	1.3	103.0	1.3	103.0	1.3
M-7	73	0.1111	2.3	20.0400	1.7	0.0162	1.5	103.3	1.6	103.3	1.6
M-8	62	0.1057	2.5	21.1325	2.1	0.0162	1.2	103.6	1.3	103.6	1.3
M-9	64	0.1090	2.0	20.5078	1.6	0.0162	1.1	103.7	1.1	103.7	1.1
M-10	63	0.1042	2.6	21.4849	2.2	0.0162	1.3	103.9	1.4	103.9	1.4
M-11	42	0.1096	2.4	20.4369	2.0	0.0163	1.4	103.9	1.4	103.9	1.4
M-12	75	0.1129	2.7	19.8669	2.4	0.0163	1.3	104.1	1.3	104.1	1.3
M-13	39	0.1066	3.5	21.0744	2.9	0.0163	2.0	104.2	2.1	104.2	2.1
M-14	55	0.1286	2.3	17.5028	1.8	0.0163	1.4	104.5	1.5	104.5	1.5
M-15	40	0.1116	3.6	20.2562	2.9	0.0164	2.1	104.9	2.2	104.9	2.2
M-16	31	0.1118	3.0	20.2741	2.5	0.0164	1.8	105.1	1.8	105.1	1.8
M-17	50	0.1149	2.2	19.7394	1.9	0.0165	1.1	105.2	1.2	105.2	1.2
M-18	129	0.1083	1.8	20.9282	1.3	0.0165	1.3	105.2	1.3	105.2	1.3
M-19	56	0.1088	2.1	20.9601	1.8	0.0165	1.2	105.8	1.3	105.8	1.3
M-20	49	0.0967	2.7	23.6100	2.3	0.0166	1.3	105.9	1.4	105.9	1.4
M-21	84	0.1054	2.4	21.6674	2.1	0.0166	1.2	105.9	1.3	105.9	1.3
M-22	36	0.1012	3.1	22.6078	2.7	0.0166	1.4	106.2	1.5	106.2	1.5
M-23	69	0.1062	2.0	21.5647	1.5	0.0166	1.3	106.2	1.3	106.2	1.3
M-35 (Granodiorite)											
M-35-1	51	0.0953	3.9	22.4853	3.6	0.0156	1.4	99.5	1.4	99.5	1.4
M-35-2	66	0.1051	2.3	20.5764	1.9	0.0157	1.3	100.4	1.3	100.4	1.3
M-35-3	63	0.1075	1.9	20.2296	1.6	0.0158	1.1	101.0	1.1	101.0	1.1
M-35-4	37	0.0954	3.1	22.8286	2.8	0.0158	1.3	101.1	1.3	101.1	1.3
M-35-5	75	0.0978	1.8	22.4135	1.5	0.0159	1.1	101.7	1.1	101.7	1.1
M-35-6	47	0.1041	2.6	21.0762	2.1	0.0159	1.5	101.9	1.5	101.9	1.5
M-35-7	70	0.1068	1.8	20.5846	1.3	0.0160	1.2	102.0	1.2	102.0	1.2
M-35-8	40	0.0921	2.8	23.9063	2.5	0.0160	1.4	102.2	1.4	102.2	1.4
M-35-9	46	0.0922	6.0	23.8704	5.9	0.0160	1.2	102.2	1.2	102.2	1.2
M-35-	48	0.1034	2.8	21.4563	2.5	0.0161	1.3	103.0	1.4	103.0	1.4
M-35-	46	0.1030	3.3	21.5735	2.9	0.0161	1.6	103.1	1.6	103.1	1.6
M-35-	92	0.1075	2.6	20.7475	1.9	0.0162	1.8	103.5	1.9	103.5	1.9
M-35-	125	0.1051	1.9	21.2219	1.3	0.0162	1.4	103.5	1.5	103.5	1.5
M-35-	45	0.1060	2.8	21.0563	2.5	0.0162	1.3	103.6	1.3	103.6	1.3
M-35-	51	0.1055	2.6	21.2623	1.7	0.0163	1.9	104.0	2.0	104.0	2.0
M-35-	92	0.1094	2.1	20.5354	1.7	0.0163	1.3	104.2	1.3	104.2	1.3
M-35-	158	0.1129	2.5	20.6839	1.9	0.0169	1.6	108.3	1.8	108.3	1.8
M-35-	617	0.1136	2.2	20.6367	0.9	0.0170	2.0	108.7	2.2	108.7	2.2
M-35-	59	0.1173	2.0	20.1533	1.6	0.0171	1.1	109.6	1.2	109.6	1.2
M-35-	47	0.1162	3.0	20.9436	2.2	0.0177	2.0	112.8	2.3	112.8	2.3
M-35-	32	0.1038	2.8	23.6088	2.2	0.0178	1.8	113.7	2.0	113.7	2.0
M-35-	346	0.1228	2.0	20.5199	1.1	0.0183	1.7	116.8	2.0	116.8	2.0
M-35-	103	0.1258	3.2	20.8276	1.7	0.0190	2.7	121.4	3.2	121.4	3.2

Mafic rocks, which are related to ophiolitic series are from the flysch complex of eastern Iran, observed in the south of the area. Intrusive bodies in the center of the study area show quartzdiorite, monzodiorite, quartz monzonite to granodiorite composition (Fig. 1). Monzodiorite is the oldest intrusive unit that is located in north-eastern part (Fig. 1). Granodiorite is the youngest intrusive bodies based on filed relationship (Fig. 1 & 2). The contacts of the intrusive rocks and carbonate rock units are mainly controlled by faults. However, based on structural control, as well as tectonic activity, limited outcrop of recrystallized limestone and low-grade metamorphic rocks are present in the margins of intrusive igneous bodies in this area (Fig. 1).

Quartz monzonite is located in the central part of the study area (Fig. 1 & 2B). This unit has a granular texture. In some thin sections, intergranular and myrmekitic textures are observed. Some space between plagioclase is occupied by pyroxene crystals. The mineral composition is comprised of 45% plagioclase, approximately 10-14% K-feldspar, 10-16% quartz, and 5-10% pyroxene and hornblende (Fig. 2D). Plagioclase is observed in the form of euhedral to subhedral crystals with apatite inclusions and most of them are oligoclase. Alkaline feldspar is found in the form of euhedral to subhedral crystals, occasionally with Carlsbad twining. Magnetite (2%), and zircon are present as accessory minerals. Alkaline feldspar is altered to sericite and kaolinite. Plagioclase is altered to sericite and in some cases to chlorite and calcite as secondary minerals. Hornblende and pyroxene are altered to chlorite and actinolite.

Monzodiorite is located in north-eastern part (Fig. 1 & 2C). The texture of this rock is hypidiomorphic to xenomorph granular but sometimes shows myrmekite texture. The main minerals are 55% plagioclase, nearly 20% K-feldspar, <5% quartz, and nearly 5% pyroxene (Fig. 2E). Magnetite (3%), apatite and zircon are the accessory minerals. Plagioclase is the most abundant mineral and its composition changes from albite to labradorite, but in general its composition is andesine. Propylitic alteration is observed in monzodiortite in a widespread range while the samples were taken from the eastern part of the area where non-altered outcrops existed. Low amounts of sericite, epidote and calcite are present in fresh rocks. Slight alteration of plagioclase to sericite and calcite, and pyroxene to epidote are observed.

Outcrop of quartz diorite is in the central part of the study area (Fig. 1 & 2B). This rock has a granular and porphyry texture. The main minerals are plagioclase 57–62%, hornblende 7–9%, K-feldspar 8–10%, pyroxene 4–5% and quartz 4–5% (Fig. 2F). Pyroxene is amorphous to euhedral sometimes with Carlsbad twining. Apatite, magnetite and zircon are the accessory minerals. This rock has experienced propylitic type alteration. The most important alteration minerals include chlorite (about 10%), carbonate (2.5%) and sericite (1–2%).

Granodiorite has a granular and sometimes granophyric texture, consisting of 45% plagioclase, 15% K-feldspar, 20% quartz, and 5–8% biotite. Other mafic minerals include 5% hornblende and 10% pyroxene (Fig. 2G). Plagioclase is the most abundant mineral and shows euhedral to subhedral shapes with polysynthetic twining. Plagioclase is mainly altered to sericite or epidote and chlorite. Alkali feldspar is often altered to kaolinite. Most of mafic minerals have subhedral forms and have altered into chlorite and calcite. Other accessory minerals are titanite, apatite, zircon and opaque minerals.

Whole rock compositions

Major elements

SiO_2 contents of intrusive rocks varies from 52.8 to 69.6 wt.% (Table 1) and plot mainly in the fields of diorite, monzodiorite and granodiorite of the Middlemost (1994) diagram (Fig. 3A) which are aligned with the results of petrography studies. In $Al_2O_3/(CaO+K_2O+Na_2O)$, and $Al_2O_3/(CaO+K_2O+Na_2O)$ versus SiO_2 diagram (Fig. 3B), the compositions primarily fall within

the metaluminous field (Shand, 1974).

Trace and rare elements

Trace elements concentrations of intrusive rock samples from the study area are presented in Table 1. Relatively flat distribution of heavy rare earth elements (HREE) as well as substantial enrichment in light rare earth elements (LREE), along with $(La/Yb)_N$ values of 4.9–6.1 in quartz-monzonite and granodiorite (Fig. 4A) and 2.61–2.79 in diorite (Fig. 4B) in the Chondrite-normalized rare earth element samples (Boynton, 1984).

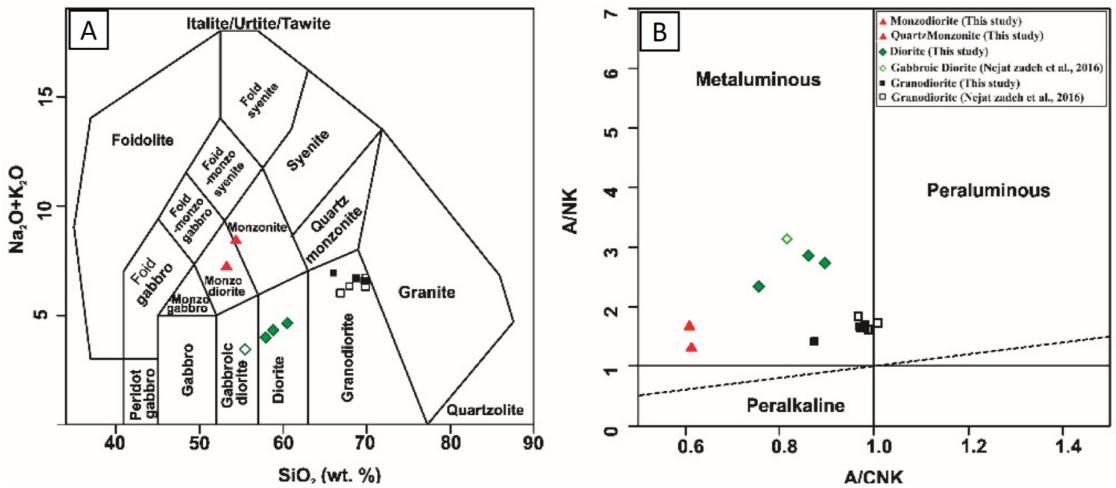

Figure 3. Geochemical classification of the Kalateh-Naser intrusive rocks (A) according to Na_2O+K_2O vs. SiO_2 (Middlemost, 1994), (B) Molecular A/CNK $[Al_2O_3/(CaO + Na_2O + K_2O)]$ vs SiO_2 (wt.%) diagram (Shand, 1974). The compositions mostly plot in the metaluminous domains

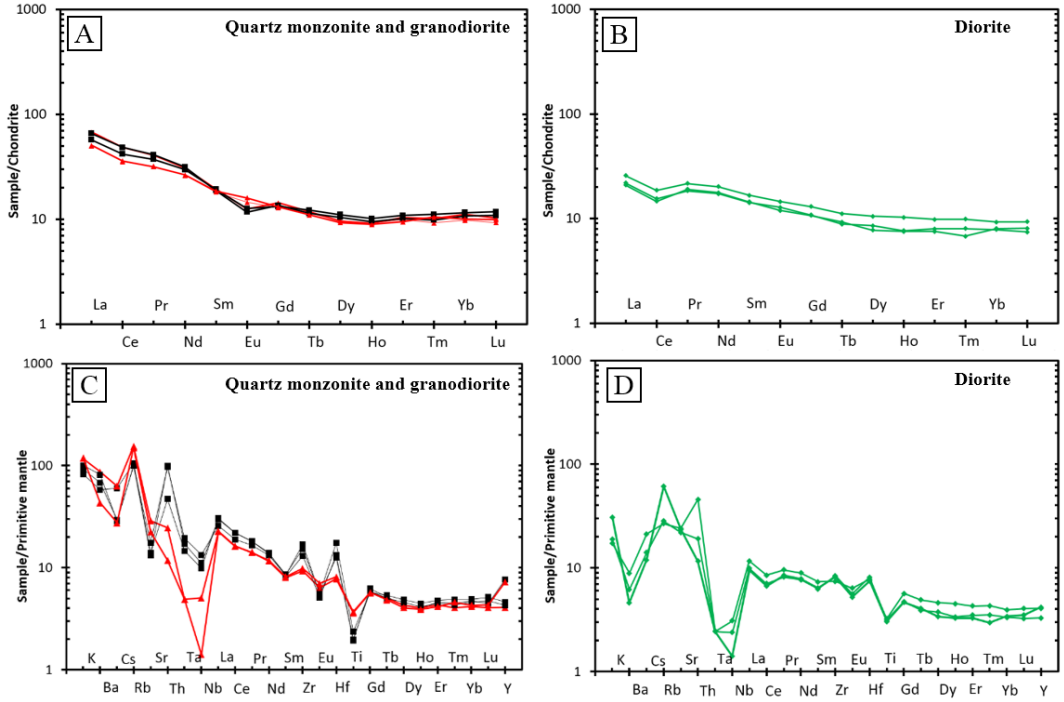

Figure 4. Chondrite-normalized (A, B) and primitive-mantle-normalized (C, D) multi-element diagrams for intrusive rocks in the Kalateh-Naser. Normalizing values are from Boynton (1984) and Sun and McDonough (1989), respectively (Symbols as Fig. 3)

The values of Gd_N/Yb_N vary from 1.1 to 1.4 (average 1.3) which manifest relatively flat heavy rare earth element (HREE) pattern on the chondrite normalized diagram (Li et al., 2013). They show enrichment of LILE compared to HFSE in the primitive mantle-normalized trace element spider diagram (Fig. 4C, D). All samples demonstrate positive anomalies in Rb, Cs, and Sr elements and negative anomalies in Ti and Nb (Fig. 4C, D). Intrusive rocks show slightly negative Eu anomalies (Eu/Eu* = 0.74–0.99; Fig. 4C, D) and concentrations of Sr (265–607.2 ppm).

Age Dating

U–Pb ages of the Kalateh-Naser intrusive igneous rocks were calculated on separated zircons from two specimens: samples (1) Quartz monzonite (sample no. M-33), and sample (2) Granodiorite (sample no. M-35-3). In both samples the size of zircon grains is fine to medium (50–150 μm), with prismatic shape and colorless. Cathodoluminescence imaging except for minor zircon crystals, confirms that most grains are not complex. Our preferred $^{207}Pb/^{206}Pb$ ages of the monzodiorite and granodiorite are = 104.23 ± 0.85 Ma (MSWD = 0.95, n=23 total spots) and 102.13 ± 0.91 Ma (MSWD=0.91, n=25), respectively. Table 2 provides a summary of ages, and Fig. 5 illustrates U–Pb Concordia diagram and weighted mean ages.

Radiogenic isotopes

Table 3 shows the results of the Rb-Sr and Sm-Nd isotopic analysis. The $^{87}Sr/^{86}Sr$ and $^{143}Nd/^{144}Nd$ ratios for monzodiorite sample are 0.70539 and 0.512796, respectively.

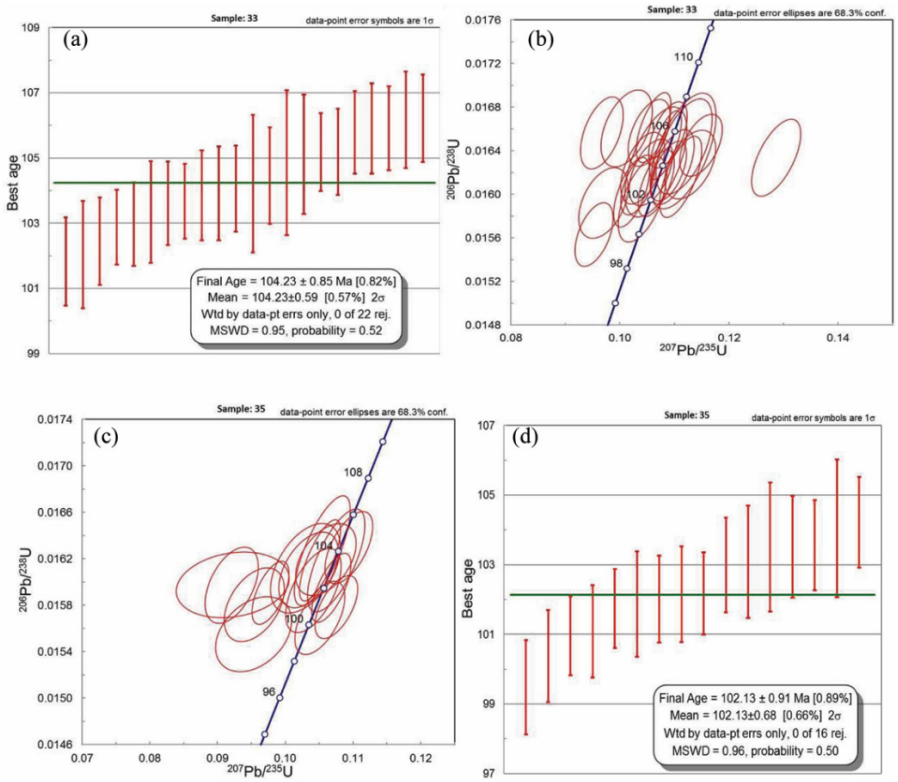

Figure 5. Zircon U-Pb plots of isotopic data (1σ confidence level) for quartz monzonite: (A) concordia diagram, and (B) average age plot. Zircon U-Pb plots of isotopic data (1σ confidence level) for Granodiorite: (C) concordia diagram, and (D) average age plot. Preferred $^{207}Pb/^{206}Pb$ ages of the monzodiorite and granodiorite are = 104.23 ± 0.85 Ma (MSWD = 0.95, n=23 total spots) and 102.13 ± 0.91 Ma (MSWD=0.91, n=25), respectively

The $^{87}Sr/^{86}Sr$ and $^{143}Nd/^{144}Nd$ ratio for granodiorite sample are 0.705161 and 0.512697, respectively. Recalculated to the age of crystallization of the monzodiorite at 104.2 Ma and granodiorite at 102 Ma, the εNd values for monzodiorite sample is 1.15, and the εNd value for granodiorite is 3.08 (Table 3). For comparison, these values along with the individual initial $^{87}Sr/^{86}Sr$ values previously published for igneous rocks from the eastern Iran are presented in Fig. 6 and Table 4. As depicted in Fig. 7. These values are higher than Bulk Earth $^{87}Sr/^{86}Sr$ and $^{143}Nd/^{144}Nd$ ratios.

Table 3. Rb-Sr and Sm-Nd isotopic data of the intrusive rocks from the Kalateh-Naser area. Errors are 2σ. Initial $^{143}Nd/^{144}Nd$ and $^{87}Sr/^{86}Sr$ ratios were calculated using the crystallizations age of 104 and 102 Ma

Sample no	Age (Ma)	Sr (ppm)	Rb (ppm)	$^{87}Sr/^{86}Sr$ measured	2σ	$^{87}Sr/^{86}Sr$ initial	Nd(ppm)	Sm(ppm)	$^{143}Nd/^{144}Nd$ measured	εNd
Monzodiorite (M-33)	104	607.2	98.6	0.705390	0.000005	0.7051	15.7	3.54	0.512796	+1.15
Granodiorite (M-35)	102	293	67	0.705161	0.000005	0.7049	18.5	3.81	0.512697	+3.08

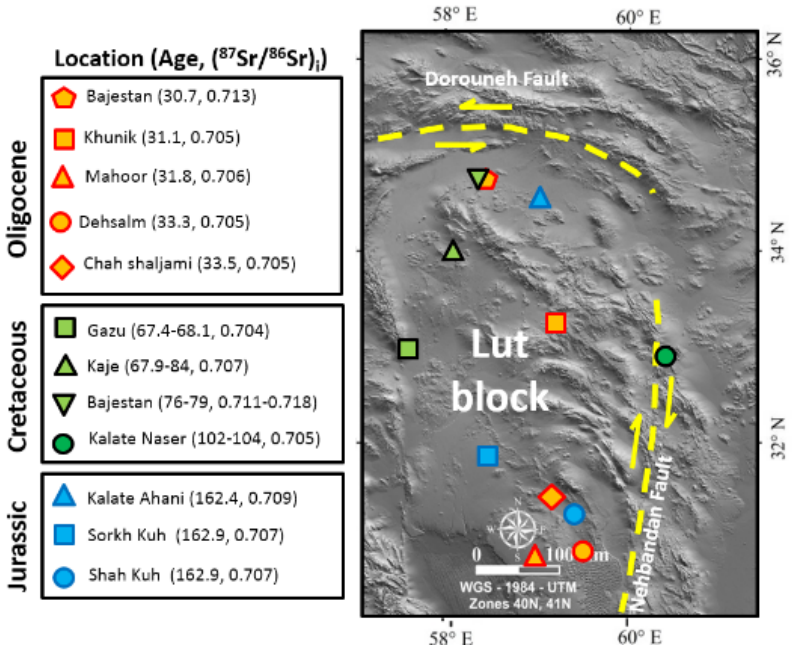

Figure 6. Location of reported granitoids with early Cretaceous (Kalateh-Naser), late Cretaceous and Jurassic ages in Lut Block (references of data as same table 4)

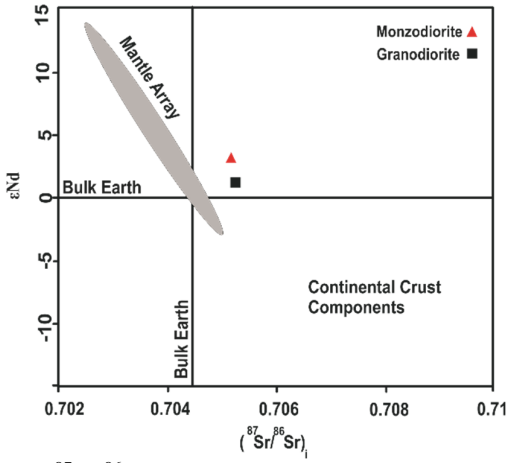

Figure 7. εNd vs. $(^{87}Sr/^{86}Sr)_i$ diagram for the Kalateh-Naser intrusive rocks

Table 4. Average Rb-Sr isotopic and age data for granitoids in the Lut block

Area	Rock Type	Age (Ma)	Granitoid Type	Tectonic Setting	$^{7}Sr/^{86}Sr$ initial	References
Bajestan	Monzogranite	30.7	S-type	SYNCLOG	0.7132	Ahmadirouhani, 2017
Khunik	Granodiorite	31.1	I-type	VAG	0.7046	Samiee et al., 2016
Mahoor	Diorite	31.8	I-type	VAG	0.7060	Miri Beydokhti et al., 2015
Dehsalm	Quartz monzonit	33.3	I-type	VAG	0.7050	Arjmandzadeh & Santos, 2014
Chah shaljami	monzonite	33.5	I-type	VAG	0.7047	Arjmandzadeh, et al., 2011
Gazu	Granodiorite	75.2	I-type	VAG	0.7045	Mahdavi et al., 2016
Kajeh	Granite to diorite	67.9-84.2	I-type	VAG	0.7072	Najafi et al., 2014
Bajestan	Granite porphyry	79	S-type	SYNCLOG	0.7109	Ahmadirouhani, 2017
	Monzogranite/ Syenogranite	76	S-type	SYNCLOG	0.7144	Ahmadirouhani, 2017
Kalateh Naser	Monzodiorite/ Granodiorite	102-104	I-type	VAG	0.7050	This study
Kalateh Ahani	Granodiorite	162.4	S-type	SYNCLOG	0.7091	Esmaeily et al., 2005
	Monzonite	109	S-type	SYNCLOG	0.7107	Karimpour et al., 2014
Sorkh Kuh	Granodiorite	162-170	S-type	SYNCLOG	0.7069	Tarkian et al., 1983; Karimpour et al. 2011
Shah Kuh	Monzogranite	163	S-type	SYNCLOG	0.7065	Esmaeily, 2001; Karimpour et al. 2011
	Syenogranite	161	S-type	SYNCLOG	0.7062	

Discussion

Crustal Contamination

The low Ti and P and the high K, Th, and Rb in the studied rocks are comparable to crustal melts and can indicate magma contamination in the upper crust during its evolution (Kuşcu et al., 2002). The Nb/La in the studied rocks is between 0.23-0.33 for quartz monzonite, 0.06-0.54 (average 0.31) for granodiorite and 0.39 for quartz diorite. The average value of Nb/U of the studied rocks is 3.4 (quartz diorite), 4.23 (granodiorite), and 5.34 (quartz monzonite). The Nb/La and Nb/U ratios is similar to the values mentioned for the upper continental crust (0.39 and 4.44 respectively; Rudnick & Gao, 2014).

It shows these rocks might be affected by upper crust. The P_2O_5/K_2O ratios in the studied rocks is between 0.03-0.1 (average 0.06) for quartz monzonite, 0.03-0.23 (average 0.09) for granodiorite, and 0.03 for quartz diorite. The P_2O_5/K_2O ratios (<0.4) also suggest that the samples from the Kalateh-Naser intrusive rocks might be affected by upper crust (Miller et al., 2000).

Fractional Crystallization

Hybrids of crustal- and mantle-derived compositions in the lower crust and subsequent fractional crystallization (Chappell et al., 2012; Zhu et al., 2015) and fractional crystallization of mantle-derived magmas in the lower crust by an underplating process (Manya & Maboko, 2016; Zhao et al., 2016, Wang et al., 2016), are thought to be the two hypotheses to generate I-type granites.

There is a reasonable fractionation trend in major and trace element abundances within the intrusive rock suite of the Kalateh-Naser (Fig. 8) which demonstrates that monzodiorite and

granodiorite could be genetically linked to a single parental magma. The possibility of simple fractional crystallization is supported by the linear trends of chemical elements, similar Sr- Nd isotopic composition and similarity of REE patterns from monzodiorite and granodiorite (Fig. 4C). Similar ages also may show that monzodiorite and granodiorite are co-magmatic, but more data (isotopic values and age dating) is needed for decision making about the source of diorite. The REE patterns of monzodiorite and granodiorite showed high degrees of REE fractionation in the Chondrite-normalized diagrams (Boynton, 1984), with strong enrichment in LREEs than diorite samples (Fig. 4A). This result is supported by the range of La_N/Yb_N values between 2.1 to 4.7 for diorite and 4.9 to 8.6 for monzodiorite and granodiorite. The studied rocks show Eu/Eu* ratios from 0.75 to 0.99 for diorite and 0.73 to 1 for monzodiorite and granodiorite. Negative Eu anomalies develop with magma differentiation due to fractional crystallization of early K-feldspar and/or plagioclase (Henderson, 1984). Also, Negative Eu anomalies may be due to partial melting of the amphibolitic lower crust and remaining of the plagioclase in the restite (Rudnick, 1992).

The plot of Th *vs.* SiO_2 (Whalen et al., 1987) is a representation of fractional crystallization process (Fig. 11A). The relationship between Ba/Sr ratio and SiO_2 (Whalen et al., 1987) shows the process of crystal fractionation in intrusive rocks (Fig. 11B). The ratio of Th/Yb and SiO_2 is sensitive to the crustal contamination in the mantle derived rocks (Taylor & Mc Lennan, 1985). The ratios of Th/Yb vs. SiO_2 in these samples show crystal fractionation associated with crustal contamination processes (Fig. 11C).

Petrogenesis

The Kalateh-Naser intrusive rock samples also exhibit weakly negative anomalies of Eu in some samples as a result of the breakdown of plagioclase due to higher mobility of Eu compared to REEs (Ling & Liu, 2002; Warmada et al., 2005).

The Ti negative anomalies can be attributed to the presence of Fe-Ti oxide minerals as remaining mineral phases in the source (Martin, 1999; Rollinson, 1993). The negative Ti anomaly can also be attributed to fractional crystallization of titanite (*e.g.,* Hoskin et al., 2000). Negative Nb is recognized as an indicator of a subduction condition and is probably related to mixing with crustal materials (Nagudi et al., 2003; Zhang et al., 2006). The negative anomaly of Nb and Ti also can indicate the involvement of continental crust rocks in magmatic processes and it is a characteristic of active continental margin zones (Wilson, 1989; Karsli et al., 2010). Depletion of Nb, Ti and P indicates the separation of titanium-bearing phases, such as ilmenite, sphene, apatite and some amphiboles.

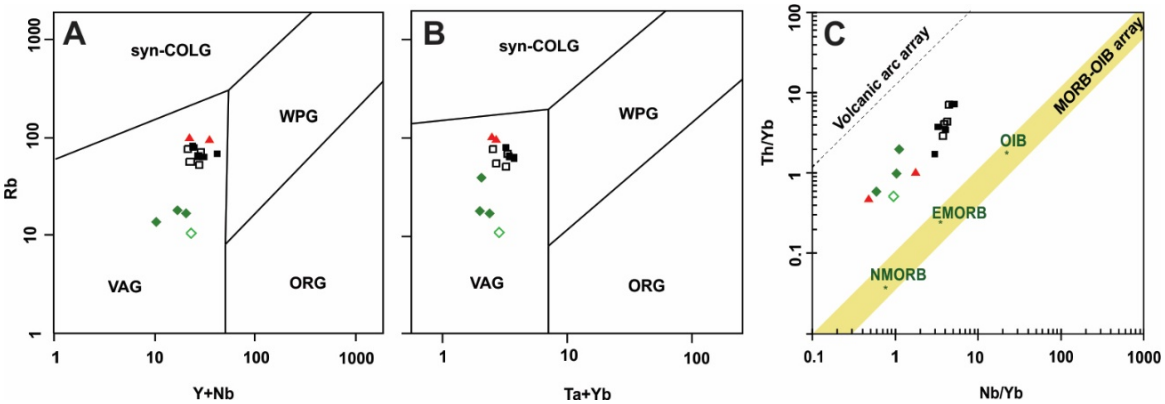

Figure 8. Tectonic discrimination diagrams of (A) Y+Nb vs. Rb and (B) Yb+Ta vs. Rb (Pearce et al. 1984), (C) Th/Yb versus Nb/Yb diagram (after Pearce, 2008), (Symbols as Fig. 3)

The samples are metaluminous and their alumina saturation (Maniar & Piccoli, 1989) remains below 0.9, and plot in I-type granitoids field (Chappell & White, 1974). Additionally, biotite, hornblende, and magnetite, that are common for I-type granites, are present in these intrusive rocks.

The plot of $Al_2O_3/(FeO_t+MgO+ TiO_2)$ vs. $Al_2O_3+ FeO_t+MgO+ TiO_2$ (Fig. 9) show domains occupied by experimental granitic liquids obtained by partial melting of metapelites, metagreywackes and amphibolites (Patiño Douce, 1999, Magna et al., 2010). Studied intrusive rocks of Kalateh-Naser area plot in amphibolite-derived melts (Fig. 9).

Furthermore, the Kalateh-Naser intrusive bodies are enriched in Rb and K, implying that they probably underwent interaction with the continental crust (e.g., Kuşcu et al., 2002). The initial $^{87}Sr/^{86}Sr$ ratio (0.7049, 0.7051) and $\varepsilon Nd_{(t)}$ values (+1.15, +3.08) for the Kalateh-Naser intrusive rocks may count of input juvenile mantle-derived magmas that had undergone mixing with upper crust. In typical upper crust K is enriched while P is depleted, which allows K/P ratio to be a distinct indicator of silicic contamination (Thompson et al., 1982). Thus, increases in K/P (8-12 for diorite and 52-64 for granodiorite) may reflect silicic upper crustal assimilation processes. The relationship between P_2O_5/K_2O, Ti/Yb *vs* Sr isotopic composition (Miller et al., 2000) for the Kalateh-Naser intrusive rocks is presented in Fig. 10.

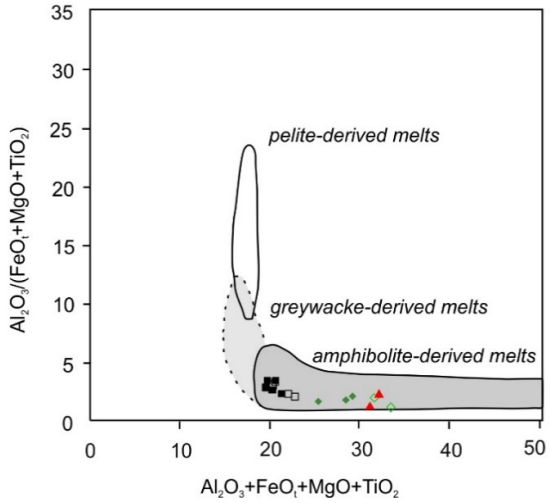

Figure 9. Plot of $Al_2O_3/(FeO_t+MgO+ TiO_2)$ vs. $Al_2O_3+ FeO_t+MgO+ TiO_2$; domains occupied by experimental granitic liquids obtained by partial melting of metapelites, metagreywackes and amphibolites (Patiño Douce, 1999, Magna et al., 2010), (Symbols as Fig. 3)

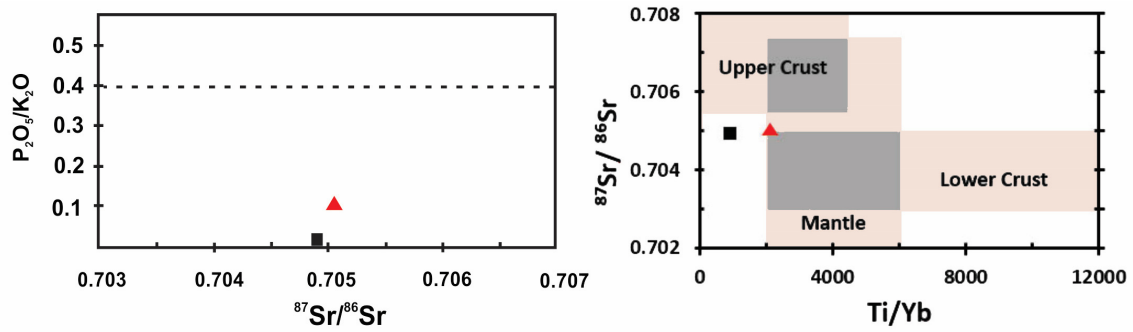

Figure 10. (A) P_2O_5/K_2O vs $^{87}Sr/^{86}Sr$, dashed line is considered to separate contaminated samples from uncontaminated ones (Miller et al., 2000). P_2O_5/K_2O (<0.4) ratios suggest that the studied samples might be affected by upper crust. (B) Relationships between Sr isotopic composition and the ratio of Ti/Yb which is sensitive to crustal contamination. Fields for common mantle, upper and lower crust (Hart, 1988) and references therein, (Symbols as Fig. 3)

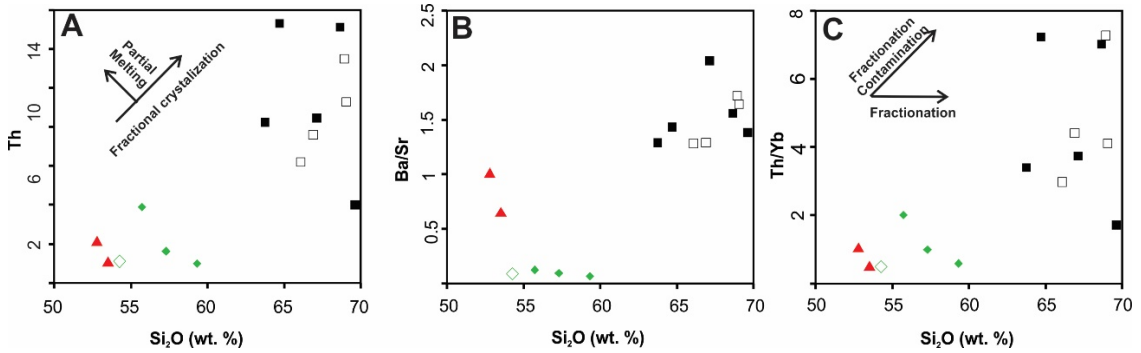

Figure 11. Diagrams showing fractional crystallization (FC) for the Kalateh-Naser intrusive rocks. (A) Th vs. SiO_2; (B) Ba/Sr vs. SiO_2 (Whalen et al., 1987); (C) Th/Yb vs. SiO_2 (Taylor and McLennan, 1985), (Symbols as Fig. 3)

The high Nb/U (1.1-7), low Ti/Yb (1080-2485) (Hart, 1988) and low P_2O_5/K_2O (<0.4) ratios suggest that the samples from the Kalate-Naser intrusive rocks might be impacted by upper crust (Fig. 10).

Samples are plotted in the VAG (Volcanic Arc Granite) zone in the Ta+Yb and Y+Nb versus Rb diagrams (Pearce et al. 1984) and in the Nb/Yb versus Th/Yb diagram (Pearce, 2008) (Fig. 8). In addition, enrichment of large ion lithophile (such as Cs, Rb, K), and strong depletion in high field strength elements (HFSE such as Nb, P, Ti) (Fig. 4B) are a typical feature of subduction related magmas in the calc-alkaline volcanic arcs (e.g., Wilson, 1989).

Based on limited available geochronology information, the first magmatic activity within the Lut block was around 160-170 million years ago (Tarkian et al., 1983; Karimpour et al., 2011; Esmaeily, 2001). The next episode of magmatism happened around 109Ma (Karimpour et al., 2011) near the north of the Lut block. Zircon U–Pb dating indicates Mid-Cretaceous age for quartz monzonite and granodiorite from the Kalateh-Naser area. Comparison of the initial $^{87}Sr/^{86}Sr$ ratio (0.7049 - 0.7051) and $^{143}Nd/^{144}Nd$ (0.512697 -0.512796) values for intrusive rocks from the Kalateh-Naser area with the other part of the Lut block demonstrate different stages and sources of magmatism in eastern Iran (Table 4 and Fig.6). For example, the initial $^{87}Sr/^{86}Sr$ ratio for Shah-Kuh and Kalate Ahani, the Jurassic granitoid rocks in the center and northwest of the Lut block, are 0.70680 and 0.70913 respectively (Esmaeily et al., 2005; Najafi et al., 2014). On the other hand, this value for granite porphyry in the Bajestan (Late Cretaceous, central Lut) is 0.710897 (Ahmadirouhani et al., 2017; Baumann et al., 1984). Widespread Tertiary magmatic activities in the Lut block also have significant differences in isotopic composition from before and after this episode (e.g., Jung et al., 1983; Abdi & Karimpour, 2013; Malekzadeh et al., 2015; Nakhaei et al., 2015; Saadat & Stern, 2012; Saadat, 2016).

Conclusion

Geochemical data of the intrusive rocks from the Kalateh-Naser area (Eastern Iran) indicate metaluminous and magnetic series magma (I- type) properties and plot in the calc-alkaline field. These intrusive rocks belong to the subduction zone in VAG category. In the Ta+Yb and Y+Nb versus Rb diagrams, all the samples have been plotted in the VAG field and in the Nb/Yb versus Th/Yb diagram also these intrusive rocks are plotted in volcanic arc field. The LREE enrichment relative to HREE and enrichment in K, Rb, Cs, Th, and U in comparison to Ti and Nb elements and the initial $^{87}Sr/^{86}Sr$ ratios show a trend toward the mantle source, contaminated by the addition of crustal materials. Zircon U–Pb dating indicates Mid-Cretaceous age for quartz monzonite and granodiorite from the Kalateh-Naser area (104.23 ± 0.85 Ma and 102.13 ± 0.91 Ma. respectively).

Comparison of the initial $^{87}Sr/^{86}Sr$ ratio (0.7049 - 0.7051) and $^{143}Nd/^{144}Nd$ (0.512697 -

0.512796) values for intrusive rocks from the Kalateh-Naser area with the other part of the Lut block demonstrate different stages and sources of magmatism in eastern Iran. Space-time isotopic composition variations indicate heterogeneous mantle and differences in amount of metsomatized mantle beneath the eastern Iran. There had been insufficient geochronological data on Cretaceous plutonic rocks in the Lut block. New geochronology information presented here, increase our knowledge related to magmatic activities during Mid-Cretaceous in eastern Iran.

Acknowledgments

This paper is a part of the first author's Ph.D. thesis at Ferdowsi University of Mashhad, Iran. We are grateful to Dr. Ghoorchi for her technical support and Madan Yaran Lut Company for giving us the opportunity to work on this project. We also want to thank anonymous reviewers for constructive comments that improved the final manuscript.

References

Abdi, M., Karimpour, M.H., 2013. Petrochemical Characteristics and Timing of Middle Eocene Granitic Magmatism in Kooh-Shah, Lut Block, Eastern Iran. Acta Geologica Sinica-English Edition, 87:1032-1044.

Ahmadirouhani, R., Karimpour, M.H., Rahimi, B., Malekzadeh-Shafaroudi, A., Klotzli, U., Santos, J.F., 2017. Petrology, geochronology, geochemistry and petrogenesis of Bajestan granitoids, North of Ferdows, Khorasan Razvi Province. Journal of Economic Geology, 8:525-552. (in Persian with English abstract)

Arjmandzadeh, R., Karimpour, M.H., Mazaheri, S.A., Santos, J.F., Medina, J.M., Homam, S.M., 2011. Sr–Nd isotope geochemistry and petrogenesis of the Chah-Shaljami granitoids (Lut block, eastern Iran). Journal of Asian Earth Sciences, 41: 283-296.

Arjmandzadeh, R., Santos, J.F., 2014. Sr–Nd isotope geochemistry and tectonomagmatic setting of the Dehsalm Cu–Mo porphyry mineralizing intrusives from Lut Block, eastern Iran. International Journal of Earth Sciences, 103: 123-140.

Baumann, A., Spies, O., Lensch, G., 1984. Strontium isotopic composition of post-ophiolitic Tertiary volcanics between Kashmar, Sabzevar and Quchan/NE Iran. Neues Jahrbuch für Geologie und Paläontologie-Abhandlungen, 409-416.

Berberian, M., King, G.C.P., 1981. Towards a paleogeography and tectonic evolution of Iran: Reply. Canadian Journal of Earth Sciences, 18: 1764-1766.

Boynton, W.V, 1984. Geochemistry of the rare earth elements: meteorite studies. In: Henderson, P. (Ed.), Rare Earth Element Geochemistry. Elsevier, Amsterdam, 63-114.

Chappell, B.W., Bryant, C.J. and Wyborn, D., 2012. Peraluminous I-type granites. Lithos, 153:142-153.

Chappell, B.W., White, A.J.R., 1974. Two contrasting granite types. Pacific Geology, 8:173-174.

Defant, M.J., Drummond, M.S., 1990. Derivation of some modern arc magmas by melting of young subducted lithosphere. Nature, 347: 662-665.

Esmaeily, D., 2001. Petrologyand geochronologyof Shah-Kuh granite with special references to tin mineralization. Ph.D. thesis, University of Tarbiat-Modarres, Tehran, 296 p. (in Persian with English abstract)

Esmaeily, D., Nédélec, A., Valizadeh, M.V., Moore, F., Cotten, J., 2005. Petrology of the Jurassic Shah-Kuh granite (eastern Iran), with reference to tin mineralization. Journal of Asian Earth Sciences, 25:961-980.

Hoskin, P.W.O., Kinny, P.D., Wyborn, D., Chappell, B.W., 2000. Identifying accessory mineral saturation during differentiation in granitoid magmas: An integrated approach. Journal of Petrology, 41:1365–1395.

Hart, S.R., 1988. Heterogeneous mantle domains: signatures, genesis and mixing chronologies. Earth and Planetary Science Letters, 90: 273-296.

Jung, D., Keller, J., Khorasani, R., Marcks, C., Baumann, A., Horn, P., 1983. Petrology of the Tertiary

magmatic activity the northern Lut area, East of Iran. Ministry of Mines and Metals, GSI, Geodynamic Project (Geotraverse) in Iran 51:285-336.

Karimpour, M.H., Malekzadeh-Shafaroudi, A., Moradi Noghondar, M., Farmer, G.L., Stern, C.R., 2014. Geology, mineralization, Rb-Sr & Sm-Nd geochemistry, and U–Pb zircon geochronology of Kalateh Ahani Cretaceous intrusive rocks, southeast Gonabad. Journal of Economic Geology, 5:267-290. (in Persian with English abstract)

Karimpour, M.H., Stern, C., Farmer, L., Saadat, S., 2011. Review of age, Rb-Sr geochemistry and petrogenesis of Jurassic to Quaternary igneous rocks in Lut Block, Eastern Iran. Geopersia, 1:19-54.

Karsli, O., Dokuz, A., Uysal, I., Aydin, F., Chen, B., Kandemir, R., Wijbrans, J., 2010. Relative contributions of crust and mantle to generation of Campanian high-K calc-alkaline I-type granitoids in a subduction setting, with special reference to the Harsit Pluton, Eastern Turkey. Contributions to Mineralogy and Petrology, 160: 467-487.

Kretz, R., 1983. Symbols for rock-forming minerals. American mineralogist, 68: 277-279.

Kuşcu, I., Kuşcu, G.G., Meinert, L.D., Floyd, P.A., 2002. Tectonic setting and petrogenesis of the Çelebi granitoid (Kırıkkale-Turkey) and comparison with world skarn granitoids. Journal of Geochemical Exploration, 76: 175-194.

Li, Y.B., Kimura, J.I., Machida, S., Ishii, T., Ishiwatari, A., Maruyama, S., Qiu, H.N., Ishikawa, T., Kato, Y., Haraguchi, S., Takahata, N., 2013. High-Mg adakite and low-Ca boninite from a Bonin fore-arc seamount: implications for the reaction between slab melts and depleted mantle. Journal of Petrology, 54:1149-1175.

Ling, Q.C., Liu, C.Q., 2002. Behavior of the REEs and other trace elements during fluid-rock interaction related to ore-forming processes of the Yinshan transitional deposit in China. Geochemical Journal, 36:443-463.

López-Moro, F.J., López-Plaza, M., Romer, R.L., 2012. Generation and emplacement of shear-related highly mobile crustal melts: the synkinematic leucogranites from the Variscan Tormes Dome, Western Spain. International Journal of Earth Sciences, 101: 1273-1298.

Magna, T., Janoušek, V., Kohút, M., Oberli, F., Wiechert, U., 2010. Fingerprinting sources of orogenic plutonic rocks from Variscan belt with lithium isotopes and possible link to subduction-related origin of some A-type granites. Chemical Geology, 274(1-2):94-107.

Mahdavi, A., Karimpour, M.H., Mao, J., Heidarian Shahri, M.R., Malekzadeh-Shafaroudi, A., Li, H., 2016. Zircon U–Pb geochronology, Hf isotopes and geochemistry of intrusive rocks in the Gazu copper deposit, Iran: Petrogenesis and geological implications. Ore Geology Reviews, 72: 818-837.

Malekzadeh, A.M., Karimpour, M.H., Stern, C.R., 2015. The Khopik porphyry copper prospect, Lut Block, Eastern Iran: geology, alteration and mineralization, fluid inclusion, and oxygen isotope studies. Ore Geology Reviews, 65: 522-544.

Maniar, P.D., Piccoli, P.M., 1989. Tectonic discrimination of granitoids. Geological society of America bulletin, 101: 635-643.

Manya, S., Maboko, M.A., 2016. Generation of Palaeoproterozoic tonalites and associated high-K granites in southwestern Tanzania by partial melting of underplated mafic crust in an intracontinental setting: Constraints from geochemical and isotopic data. Lithos, 260: 120-133.

Martin, H., 1999. Adakitic magmas: modern analogues of Archaean granitoids. Lithos, 46: 411-429.

Middlemost, E.A., 1994. Naming materials in the magma/igneous rock system. Earth-science reviews, 37: 215-224.

Miller, J.S., Glazner, A.F., Farmer, G.L., Suayah, I.B., Keith, L.A., 2000. A Sr, Nd, and Pb isotopic study of mantle domains and crustal structure from Miocene volcanic rocks in the Mojave Desert, California. Geological Society of America Bulletin, 112: 1264-1279.

Miri-Beydokhti, R.M., Karimpour, M.H., Mazaheri, S.A., Santos, J.F., Klötzli, U., 2015. U–Pb zircon geochronology, Sr–Nd geochemistry, petrogenesis and tectonic setting of Mahoor granitoid rocks (Lut Block, Eastern Iran). Journal of Asian Earth Sciences, 111: 192-205.

Nagudi, B., Koeberl, C., Kurat, G., 2003. Petrography and geochemistry of the Singo granite, Uganda, and implications for its origin. Journal of African Earth Sciences, 36:73-87.

Najafi, A., Karimpour, M.H., Ghaderi, M., Stern, C.R., Farmer, J.L., 2014. Zircon U–Pb geochronology, isotope geochemistry of Rb–Sr and Sm–Nd and petrogenesis of granitoid intrusive rocks in Kajeh exploration area, northwest of Ferdows: evidence for Late Cretaceous magmatism in the Lut block. Journal of Economic Geology, 6: 107-135. (in Persian with English abstract).

Nakhaei, M., Mazaheri, S.A., Karimpour, M.H., Stern, C.R., Zarrinkoub, M.H., Mohammadi, S.S., 2015. Geochronologic, geochemical, and isotopic constraints on petrogenesis of the dioritic rocks associated with Fe skarn in the Bisheh area, Eastern Iran. Arabian Journal of Geosciences, 8: 8481-8495.

Nejatzadeh, M.J., Homam, M., Saadat, S., 2016. Geochemical studies of intrusive rocks of Kalateh Naser area, southern Khorasan, in Proceedings, Iranian Society of Economic geology symposium, 9th, Birjand, Iran University of Birjand, p.1-8. (in Persian with English abstract).

Pang, K.N., Chung, S.L., Zarrinkoub, M.H., Khatib, M.M., Mohammadi, S.S., Chiu, H.Y., Chu, C.H., Lee, H.Y., Lo, C.H., 2013. Eocene–Oligocene post-collisional magmatism in the Lut–Sistan region, eastern Iran: Magma genesis and tectonic implications. Lithos, 180: 234-251.

Patiño Douce, A.E., 1999. What do experiments tell us about relative contributions of crust and mantle to the origin of granitic magmas?. In: Castro, A., Fernández, C., Vigneresse, J.L. (Eds.), Understanding Granites: Integrating New and Classical Techniques. Geological Society of London Special Publications, London, 168: 55-75.

Pearce, J.A., 2008. Geochemical fingerprinting of oceanic basalts with applications to ophiolite classification and the search for Archean oceanic crust. Lithos, 100: 14-48.

Pearce, J.A., Harris, N.B., Tindle, A.G., 1984. Trace element discrimination diagrams for the tectonic interpretation of granitic rocks. Journal of petrology, 25: 956-983.

Pin, C., Gannoun, A., Dupont, A., 2014. Rapid, simultaneous separation of Sr, Pb, and Nd by extraction chromatography prior to isotope ratios determination by TIMS and MC-ICP-MS. Journal of Analytical Atomic Spectrometry, 29: 1858-1870.

Rollinson, H.R., 1993, Using geochemical data: evaluation, presentation, interpretation: Harlow, Essex, England: New York: Longman Scientific & Technical, 352 pp.

Rudnick, R.L., 1992. Restites, Eu anomalies and the lower continental crust. Geochimica et Cosmochimica Acta, 56(3): 963-970.

Rudnick, R.L., Gao, S., 2014. Composition of the continental crust. Treatise on geochemistry. Amestradam: Elsevier. 64: 1-64.

Saadat, S., 2016. Geology, Geochemistry and Ground Magnetic Survey on Kalateh Naser Iron Ore Deposit, Khorasan Jonoubi Province. Journal of Economic Geology, 8: 593-607, (in Persian with English abstract)

Saadat, S., Stern, C., 2016. Distribution and geochemical variations among paleogene volcanic rocks from the north-central Lut block, eastern Iran. Iranian Journal of Earth Sciences, 8(1): 1-24.

Saadat, S., Stern, C.R., 2011. Petrochemistry and genesis of olivine basalts from small monogenetic cones of Bazman stratovolcano, Makran arc, southeastern Iran. Lithos, 125: 607–619.

Saadat, S., Stern, C.R., 2012. Petrochemistry of a xenolith-bearing Neogene alkali olivine basalt from northeastern Iran. Journal of Volcanology and Geothermal Research, 225: 13-29.

Saccani, E., Delavari, M., Beccaluva, L., Amini, S., 2010. Petrological and geochemical constraints on the origin of the Nehbandan ophiolitic complex (eastern Iran). Implication for the evolution of the Sistan Ocean. Lithos, 117: 209-228.

Samiee, S., Karimpour, M.H., Ghaderi, M., Heidarian Shahri, M.R., Klöetzli, U., Santos, J.F., 2016. Petrogenesis of subvolcanic rocks from the Khunik prospecting area, south of Birjand, Iran: Geochemical, Sr–Nd isotopic and U–Pb zircon constraints. Journal of Asian Earth Sciences, 115: 170-182.

Shahabpour, J., 2005. Tectonic evolution of the orogenic belt in the region located between Kerman and Neyriz. Journal of Asian Earth Sciences, 24: 405-417.

Shand, S.J., 1974. Eruptive rocks; their genesis, composition, classification, and their relation to ore deposits, with a chapter on meteorites. Revised second edition, New York, Hafner Publishing Company, 350 pp.

Sun, S.S., McDonough, W.F., 1989. Chemical and isotopic systematics of oceanic basalts: implications for mantle composition and processes. Geological Society, London, Special Publications, 42: 313-345.

Tanaka, T., et al., 2000. JNdi-1: a neodymium isotopic reference in consistency with LaJolla neodymium. Chemical Geology, 168: 279-281.

Tarkian, M., Bock, W.D., Neumann, M., 1983. Geology and mineralogy of the Cu− Ni− Co− U ore deposits at Talmessi and Meeskani, central Iran. Tschermaks mineralogische und petrographische

Mitteilungen, 32: 111-133.
Taylor, S.R., McLennan, S.M., 1985. The continental crust: Its composition and evolution. Blackwell Scientific Publications, 312 pp.
Thompson, R.N., Dickin, A.P., Gibson, I.L., Morrison, M.A., 1982. Elemental fingerprints of isotopic contamination of Hebridean Palaeocene mantle-derived magmas by Archaean sial. Contributions to Mineralogy and Petrology, 79(2): 159-168.
Tirrul, R., Bell, I.R., Griffis, R.J., Camp, V.E., 1983. The Sistan suture zone of eastern Iran. Geological Society of America Bulletin, 94: 134-150.
Wang, G.C., Jiang, Y.H., Liu, Z., Ni, C.Y., Qing, L., Zhang, Q., Zhu, S.Q., 2016. Multiple origins for the Middle Jurassic to Early Cretaceous high-K calc-alkaline I-type granites in northwestern Fujian province, SE China and tectonic implications. Lithos, 246: 197-211.
Warmada, I.W., Soe, M.T., Sinomiya, J., Setijadji, L.D., Imai, A., Watanabe, K., 2005. Petrology and geochemistry of intrusive rocks from Selogiri area, Central Java, Indonesia. In: Proceedings, Earth Resources Engineering and Geological Engineering Symposium, 2nd, Bangkok, Thailand, pp.163-169.
Whalen, J.B., Currie, K.L., Chappell, B.W., 1987. A-type granites: geochemical characteristics, discrimination and petrogenesis. Contributions to mineralogy and petrology, 95: 407-419.
Wilson, M., 1989. Igneous Petrogenesis: A global tectonic approach. Harper Collins Academic, 466 pp.
Zarrinkoub, M.H., Pang, K.N., Chung, S.L., Khatib, M.M., Mohammadi, S.S., Chiu, H.Y., Lee, H.Y., 2012. Zircon U–Pb age and geochemical constraints on the origin of the Birjand ophiolite, Sistan suture zone, eastern Iran. Lithos, 154: 392-405.
Zhang, K.J., Cai, J.X., Zhang, Y.X., Zhao, T.P., 2006. Eclogites from central Qiangtang, northern Tibet (China) and tectonic implications. Earth and Planetary Science Letters, 245: 722-729.
Zhao, J.L., Qiu, J.S., Liu, L., Wang, R.Q., 2016. The Late Cretaceous I-and A-type granite association of southeast China: Implications for the origin and evolution of post-collisional extensional magmatism. Lithos, 240: 16-33.
Zhu, R.Z., Lai, S.C., Qin, J.F., Zhao, S.W., 2015. Early-Cretaceous highly fractionated I-type granites from the northern Tengchong block, western Yunnan, SW China: Petrogenesis and tectonic implications. Journal of Asian Earth Sciences, 100: 145-163.

This article is an open-access article distributed under the terms and conditions of the Creative Commons Attribution (CC-BY) license.